

Testing Colour-magnitude Pattern as A Method in the Search for Changing-Look AGNs

Li-Tao Zhu¹, Zhongxiang Wang^{1,2*}, P. U. Devanand^{3,4}, Alok C. Gupta³, Karan Dogra^{3,4}, Jie Li^{5,6}

Ju-Jia Zhang^{7,8}, Shun-Hao Ji¹, Si-Si Sun¹

¹Department of Astronomy, School of Physics and Astronomy, Yunnan University, Kunming 650091, China; wangzx20@ynu.edu.cn

²Shanghai Astronomical Observatory, Chinese Academy of Sciences, Shanghai 200030, China

³Aryabhata Research Institute of Observational Sciences (ARIES), Manora Peak, Nainital-263001, India

⁴Department of Applied Physics/Physics, Mahatma Jyotiba Phule Rohilkhand University, Bareilly-243006, India

⁵Key Laboratory for Research in Galaxies and Cosmology, Department of Astronomy, University of Science and Technology of China, Hefei 230036, China

⁶School of Astronomy and Space Science, University of Science and Technology of China, Hefei 230026, China

⁷Yunnan Observatories, Chinese Academy of Sciences, Kunming 650216, China

⁸Key Laboratory for the Structure and Evolution of Celestial Objects, Chinese Academy of Sciences, Kunming 650216, China

Accepted XXX. Received YYY; in original form ZZZ

ABSTRACT

We develop a simple method to search for changing-look (CL) active galactic nucleus (AGN) candidates, and conduct a test run. In this method, optical variations of AGNs are monitored and CL-AGNs may appear to have a pattern of being bluer when in brightening flare-like events. Applying this method, previously-classified type 2 AGNs that show the bluer-when-brighter (BWB) pattern are selected. Among more than ten thousands type 2 AGNs classified in the Sloan Digital Sky Survey (SDSS), we find 73 candidates with possibly the strongest BWB pattern. We note that 13 of them have previously been reported as CL-AGNs. We have observed nine candidates, and found that five among them showed the CL transition from type 2 to type 1. In addition, we also test extending the selection to previously-classified type 1 AGNs in the SDSS by finding sources with a possible redder-when-brighter pattern, but none of the three sources observed by us is found to show the transition from type 1 to type 2. We discuss the variation properties in both the success and failure cases, and plan to observe more candidates selected with the method. From the observational results, a detailed comparison between the CL-AGNs and none CL-AGNs will help quantitatively refine the selection criteria and in turn allow us to configure the general properties of CLAGNs.

Key words: galaxies: active — quasars: emission lines

1 INTRODUCTION

Active Galactic Nuclei (AGNs) are among the most luminous and dynamic objects in the universe, powered by accretion onto super-massive black holes (SMBHs) at the centers of galaxies. A unification scheme for understanding AGNs' appearances, structural components, and physical properties has been established since the late 1980s (e.g., Lawrence 1987; Antonucci 1993; Urry & Padovani 1995; Tadhunter 2008). In the unified model, there are mainly two types of AGNs, type 1 and type 2, whose classifications depend on whether or not we can view the central engine and the broad-line region (BLR) and consequently on whether or not broad emission lines (BELs) are observed. Type 1 AGNs typically exhibit prominent broad ($\gtrsim 1000 \text{ km s}^{-1}$) emission lines in their optical and ultraviolet (UV) emission, while type 2 AGNs only

show narrow lines ($< 1000 \text{ km s}^{-1}$). There are also types 1.2, 1.5, 1.8, and 1.9 (Winkler 1992), classified based on the ratio of the strength of $H\beta$ to that of $[O III] 5007$; the weaker the $H\beta$ line, the higher the type number. The unified model has stood as the framework for AGNs, withstanding numerous tests and supported by a multitude of observational evidence. However, recent observations of the Changing-Look phenomenon in AGNs show challenges or at least raise questions about the unified model.

The so-called changing-look (CL) may be simply characterized by appearances or disappearances of BELs in optical/UV spectra taken at different epochs (e.g., Tohline & Osterbrock 1976; Cohen et al. 1986; Storchi-Bergmann et al. 1993; Aretxaga et al. 1999; Eracleous & Halpern 2001; Denney et al. 2014; Shappee et al. 2014; LaMassa et al. 2015). The drastic changes in BELs would indicate AGN type transitions between type 1 and type 2 or other intermediate types. The thus-found CL AGNs (CLAGNs)

* E-mail: wangzx20@ynu.edu.cn

may also be referred to as changing-state AGNs (CSAGNs; [Graham et al. 2020](#); [Ricci & Trakhtenbrot 2022](#)) in order to distinguish them from those found in X-rays, the changing-obscuration AGNs (COAGNs; for details about the latter, see, e.g., [Mereghetti et al. 2021](#); [Ricci & Trakhtenbrot 2022](#)). In the optical/UV, discoveries of many CLAGNs are enabled by the Sloan Digital Sky Survey (SDSS) and typical timescales of the CL activities are $< 10\text{--}20$ yr, limited by the taking times of at least two spectra for comparison. Extreme cases of monthly CL timescales have also been found (e.g., [Trakhtenbrot et al. 2019](#); [Katebi et al. 2019](#); [Zeltyn et al. 2022](#)). How to explain such short changing timescales in the unified model becomes a problem to be discussed, as intrinsic changes in the accretion of AGNs should follow the viscous timescale of the accretion disc, which would be of the order of $\sim 10^4$ yr (see discussion in, e.g., [MacLeod et al. 2016a](#); [Ross et al. 2018](#); [Noda & Done 2018](#); [Ruan et al. 2019](#)). Different possible scenarios have been proposed, such as changes in the innermost regions of the accretion disc on the thermal and heating/cooling front timescales ([Stern et al. 2018](#)), magnetically supported thick disc ([Dexter & Begelman 2019](#)), magnetic accretion disc with outflows ([Feng et al. 2021](#)), or radiation pressure instability occurring in the narrow ring between the outer standard disc and the inner advection-dominated accretion flow (ADAF; [Sniegowska et al. 2020](#)).

To understand the physical processes that produce the CL phenomenon, properties and distinctions of CLAGNs should be thoroughly probed. Efforts have been made to find more CLAGNs and build a large sample for property studies (e.g., [Ruan et al. 2016](#); [Runnoe et al. 2016](#); [Gezari et al. 2017](#); [Yang et al. 2018](#); [Ross et al. 2020](#); [Zhu et al. 2024](#)). There are roughly two types of methods used for systematically searching for CLAGNs, spectrum-based and light-curve-based. The first involves comparing spectra obtained from either the same survey (e.g., [Green et al. 2022](#); [Zeltyn et al. 2024](#)) or from different surveys (e.g., [Yang et al. 2018](#); [Dong et al. 2024](#); [Guo et al. 2024b,a](#)). This type can quickly and efficiently identify CLAGNs, but may also miss many of them because the results are highly dependent on the plans of the spectroscopy surveys and these surveys are time consuming. The second one tries to draw characteristics of AGN variabilities, identify the candidate CLAGNs through certain selection criteria in optical (e.g., [MacLeod et al. 2016b](#); [Frederick et al. 2019](#); [Graham et al. 2020](#); [López-Navas et al. 2022, 2023a](#); [Wang et al. 2024](#)) or infrared (e.g., [Sheng et al. 2020](#); [Wang et al. 2023](#)), in some of which the machine learning techniques are applied, and follow with spectroscopic confirmation. This type is enabled by the availability of rich amounts of light-curve data at multi-bands from different photometric surveys.

In our initial study of AGN variation patterns, we found four CLAGNs ([Zhu et al. 2024](#)), and realized that they likely shared a similar pattern of being bluer when in brightening flare-like events. This type of bluer-when-brighter (BWB) behaviour has been known in AGNs and was noticed in CLAGNs (see [Yang et al. 2018](#) and references therein). These variations are often seen in type 1 AGNs, but not in type 2s, since the latter typically have weak variations. Sources showing a BWB pattern among type 2 AGNs might have undergone the CL transitions. We thus conducted a follow-up study to explore a method of finding CLAGNs with the BWB

pattern. We essentially went through type 2 AGNs identified in the SDSS database and selected those with stronger BWB variations as the targets for finding CLAGNs. It should be pointed out that our method relies on the recent light-curve data provided by large photometric surveys, and the CL transitions could occur recently, thus reflected by the data. In this reported work, we obtained spectra for nine targets, and five of them have been identified as CLAGNs. Among the identified, three are newly discovered and two were reported in [Wang et al. \(2024\)](#). The latter two are J1020+2437 and J1150+3503 (see Table 1); our spectroscopic observations were conducted before the appearance of [Wang et al. \(2024\)](#) and we were not aware of the identification at the time. In addition, we also selected a few type 1 AGNs to test if their non-BWB behaviour would indicate the transition from type 1 to type 2. We observed three of the selected sources.

We report our observational results in this paper. In Section 2, we describe the target selection method. In Section 3, we provide information for our spectroscopic observations with the 2.4-m LiJiang Telescope (LJT, [Wang et al. 2019](#)) and the 3.6-m Devasthal Optical Telescope (DOT, [Kumar et al. 2018](#)) and the related data reduction process. We present the analysis of the photometric data and spectra for nine type-2 and three type-1 targets and the identification of 5 CLAGNs in Section 4. The results are discussed and summarized in Section 5. Throughout this paper, we adopted cosmological parameters from the Planck mission ([Planck Collaboration et al. 2020](#)), with $H_0 = 67 \text{ km s}^{-1} \text{ Mpc}^{-1}$ and $\Omega_m = 0.32$.

2 TARGET SELECTION METHOD

2.1 Archival data

Different archival photometric data were used in the target selection (Section 2.2) and analysis (Section 4). The majority of data used were from the Zwicky Transient Facility survey (ZTF; [Bellm et al. 2019](#)). The magnitude data at its z_g - and z_r -band for the sources mentioned in this work were obtained. When querying the ZTF data, we set `catflags = 0` and `chi < 4` in order to construct clean and high-quality light curves for the sources.

For our targets studied in detail, we also used the V -band magnitude data from the Catalina Real-time Transient Survey (CRTS; [Drake et al. 2009](#)) and data at the cyan (420–650 nm; ac) and orange (560–820 nm; ao) bands from the Asteroid Terrestrial-impact Last Alert System (ATLAS; [Tonry et al. 2018](#)). The ATLAS's two wide bands cover the wavelength ranges of the SDSS's $g + r$ and $r + i$ bands, respectively. In addition, the mid-infrared (MIR) data obtained from the post-cryogenic phase survey of the Wide-field Infrared Survey Explorer (WISE; [Wright et al. 2010](#)) were included. The magnitude data are at two bands, W1 ($3.4 \mu\text{m}$) and W2 ($4.6 \mu\text{m}$).

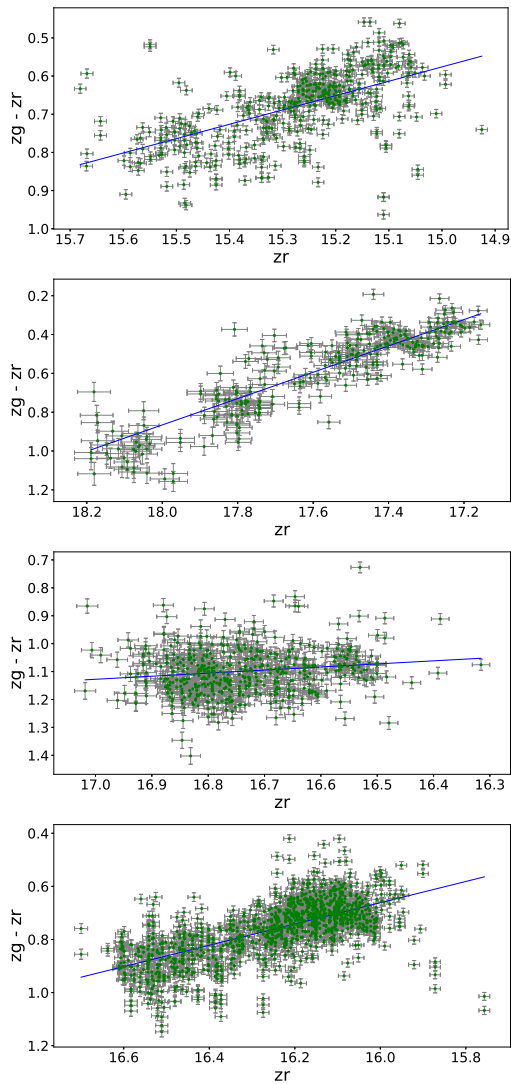


Figure 1. Colour-magnitude diagrams for the four CLAGNs reported in this work. From *top to bottom*: J0751+4948, J1020+2437, J1203+6053, and J1344+5126. Their k values determined from a linear fit (solid line in each panel) are respectively 0.376 ± 0.004 , 0.679 ± 0.008 , 0.110 ± 0.009 , and 0.401 ± 0.003 .

2.2 Target selection

We used the SQL query tool of the SDSS SkyServer¹ have decent spectra that cover the H α and H β BELs, we further required a median signal-to-noise ratio `snmedian` greater than 10 and a redshift (z) less than 0.5. In total, we obtained 16,919 spectra (without counting multiple spectra of the same sources). For the AGNs, we selected those with ZTF data points at zr -band greater than 43. This requirement was set in order to have light curves with sufficient data points for colour-magnitude (CM) analysis, and the number 43 was read from the distribution of the ZTF data points for the AGNs.

¹ <https://skyserver.sdss.org/dr16/en/tools/search/sql.aspx> to extract spectral data from the SDSS's Data Release 16 (DR16; Ahumada et al. 2020) for sources classified as 'galaxy' with subclass 'AGN'. These sources are considered as type 2 AGNs in the database. In order to

Using the z_g - and z_r -band data, we calculated the colour $z_g - z_r$, where we required the magnitudes at the two bands in the calculation be taken within one day. We obtained the CM ($z_g - z_r$ versus z_r) diagrams for each AGN; examples of the CM diagrams are shown in Figure 1. We then fit the CM data points with a linear function of $z_g - z_r = k \times z_r + c$, where k is the slope and c is a constant. The distribution of the k values obtained for more than ten thousands type 2 AGNs is shown in Figure 2. We noted that many of the k values were erroneous, resulting in unreal BWB patterns, because some sporadic variations induced the fitting results. In any case, the distribution can serve as a tool for initial source selection. As a starting point, we chose $k \geq 0.1$ as a threshold and found there were 177 sources, approximately 1.4% of the type 2 AGNs shown in Fig. 2 (compared to $\sim 34\%$ of the type 1 AGNs with $k \geq 0.1$ in the figure). After examining the CM diagrams by eye, we finally found 73 sources with clear BWB variations. Upon the starting of this work, 13 of the 73 sources have been reported as CLAGNs, already affirming the efficiency of our method in identifying CLAGN candidates from type 2 to type 1. In our spectroscopy identification (Section 3), we observed nine of the 60 candidates. The basic information for the observed sources, including their maximum optical and MIR magnitude changes (Δz_g , Δz_r , $\Delta W1$, and $\Delta W2$), is given in Table 1.²

As a test, we also conducted a similar analysis to type 1 AGNs in the SDSS database. Sources with spectra classified as 'QSO' in the SDSS DR16 database were selected, while the same criteria as those for the Type 2 AGNs were applied to the source selection. In total, we retrieved 19,023 spectra. Among them, we selected those with ZTF zr data points greater than 70. Their k -value distribution is shown in Figure 2. The idea is that these type 1 AGNs with negative k values would have a redder-when-brighter pattern, which is inconsistent with their type. This contradiction would suggest that they had the CL from type 1 to type 2. We selected a few sources with $k \leq -0.7$ as targets; in our samples, there were $\sim 2.7\%$ type 2 AGNs and $\sim 8.9\%$ type 1 AGNs satisfying the selection condition. Three of them were observed in last year's observing run.

3 LJT AND DOT OBSERVATIONS

3.1 Spectroscopy

Among the selected AGN sources (Section 2.2), we chose our targets mainly based on their visibility and brightnesses; LJT and DOT both have a limiting magnitude of approximately 19 for spectroscopic observations. The information for the targets and observations is provided in Table 2. Nine type 2 AGNs and three type 1 AGNs were observed. For LJT observations, the instrument used was the Yunnan Faint Object Spectrograph and Camera (YFOSC). This instrument has a 2048×4096 pixel² back-illuminated Charge-Coupled Device (CCD), with a pixel scale of 0.283 arcsec pixel⁻¹. The grism used was G3, which provides a wavelength coverage of 340–910 nm and a spectral dispersion of 0.29 nm pixel⁻¹. We chose

² In calculating $\Delta W1$ and $\Delta W2$, 1–2 obvious outliers of each MIR light curve were excluded, which could cause erratic results.

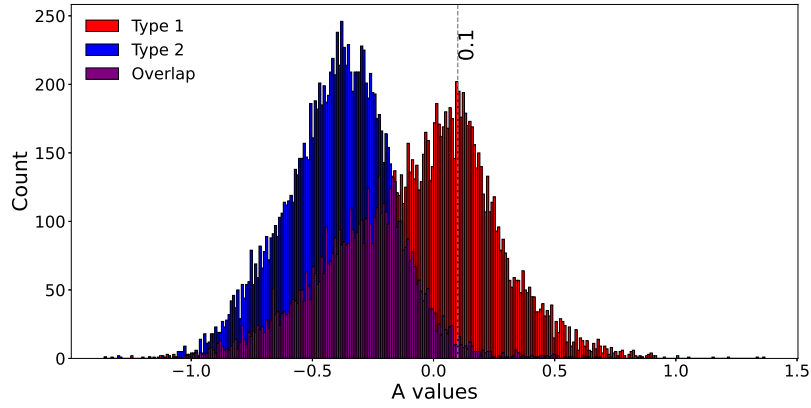


Figure 2. Distributions of the k values (the slopes) of the linear fits to each AGN's CM variation data points. A dashed line at $k = 0.1$ is drawn, type 2 AGNs above which are checked as potential CLAGN candidates.

Table 1. Basic informations of all observed sources

Target	R.A. (J2000)	Decl. (J2000)	z	Δz_g	Δz_r	$\Delta W1$	$\Delta W2$	k
Confirmed changing-look AGN								
J0751+4948	07 ^h 51 ^m 51 ^s .89	+49°48′51″.54	0.0244	1.127±0.013	0.870±0.011	0.940±0.021	1.264±0.025	0.376±0.004
J1020+2437*	10 ^h 20 ^m 38 ^s .50	+24°37′08″.35	0.1894	1.859±0.048	1.227±0.031	1.167±0.043	1.363±0.069	0.679±0.008
J1150+3503*	11 ^h 50 ^m 00 ^s .57	+35°03′56″.71	0.0611	1.102±0.024	1.358±0.020	0.492±0.035	0.922±0.061	0.20±0.01
J1203+6053	12 ^h 03 ^m 49 ^s .21	+60°53′17″.45	0.0655	0.994±0.032	0.774±0.018	0.514±0.020	0.535±0.022	0.11±0.01
J1344+5126	13 ^h 44 ^m 19 ^s .60	+51°26′24″.66	0.0629	1.328±0.021	0.970±0.014	0.825±0.026	1.019±0.035	0.401±0.003
Other candidate								
J1053+4929	10 ^h 53 ^m 44 ^s .13	+49°29′55″.99	0.1404	0.892±0.023	0.648±0.019	0.476±0.031	0.618±0.060	0.14±0.01
J1246−0156	12 ^h 46 ^m 22 ^s .70	−01°56′28″.49	0.0844	0.894±0.028	0.591±0.020	0.589±0.037	0.955±0.079	0.46±0.03
J1252+0717	12 ^h 52 ^m 52 ^s .61	+07°17′57″.67	0.1082	0.548±0.026	0.449±0.021	0.778±0.046	1.25±0.13	0.34±0.04
J1423+2454	14 ^h 23 ^m 52 ^s .09	+24°54′17″.14	0.0744	0.828±0.025	0.564±0.020	0.948±0.043	1.488±0.085	0.679±0.008
Type 1 AGN								
J1127+2654	11 ^h 27 ^m 36 ^s .38	+26°54′50″.55	0.3792	0.160±0.020	0.160±0.020	0.303±0.044	0.345±0.038	−0.758±0.001
J1527+2233	15 ^h 27 ^m 57 ^s .67	+22°33′04″.02	0.2539	0.148±0.016	0.148±0.016	0.312±0.029	0.368±0.038	−0.748±0.001
J1606+2903	16 ^h 06 ^m 28 ^s .07	+26°29′03″.83	0.4342	0.424±0.030	0.281±0.023	-	-	−0.865±0.001

* marks the two sources identified as CLAGN in Wang et al. (2024).

Table 2. Information of spectroscopic observations with LJT and DOT

Target	Telescope	Date	Exposure (sec)	Seeing (arcsec)	Standard
Confirmed changing-look AGN					
J0751+4948	LJT	2024-03-18	600	1.5	BD+33d2642
J1020+2437	LJT	2024-03-18	2000	1.5	BD+33d2642
J1150+3503	DOT	2024-03-15	1260	1.5	Feige66
J1203+6053	DOT	2024-03-15	1440	1.5	Feige66
J1344+5126	LJT	2024-03-17	1600	1.8	Feige66
Other candidate					
J1053+4929	DOT	2024-03-15	1800	1.5	Feige66
J1246−0156	LJT	2024-03-18	1800	1.5	BD+33d2642
J1252+0717	LJT	2024-03-17	2000	1.9	Feige66
J1423+2454	LJT	2024-03-18	2100	1.5	BD+33d2642
Type 1 AGN					
J1127+2654	LJT	2024-03-18	1500	1.6	BD+33d2642
J1527+2233	LJT	2024-03-18	1200	1.5	BD+33d2642
J1606+2903	LJT	2024-03-18	900	1.6	BD+33d2642

a long slit with a width of 2.5 arcsec in all exposures. In addition, spectra for wavelength and flux calibrations were also taken, which were those of a He-Ne lamp and a spectrophotometric standard, respectively.

We also conducted spectroscopic observations of three

sources using DOT. The instrument was the ARIES-Devasthal Faint Object Spectrograph and Camera (AD-FOSC), whose detector is a $4\text{k} \times 4\text{k}$ pixel² CCD. For all exposures, we chose the 132R-600 gr/mm grism, which provides a spectral dispersion of $0.10 \text{ nm pixel}^{-1}$ and a wavelength cov-

erage of 350–700 nm. The slit used was 8-arcmin long, with a width of 2.0 arcsec. Wavelength and flux calibrations were performed by taking the spectra of Neon and Argon and the spectra of a spectrophotometric standard, respectively. Because the guiding system of the telescope was not functioning, it was suggested that one exposure be a maximum of 600 sec. The exposures of the three sources given in Table 2 consist of 2–3 \leq 600 sec exposures.

3.2 Data reduction

We used the IRAF tasks for data reduction. The spectrum images were bias subtracted and flat fielded. Spectra of the sources were extracted, to which wavelength and flux calibrations were conducted. For the DOT observations, we obtained the final spectrum of each source by averaging 2–3 spectra, respectively extracted from the \leq 600 sec exposures.

4 ANALYSIS AND RESULTS

Among the nine targets selected from type 2 AGNs, three of which, J0751+4948, J1020+2437, and J1344+5126, should be type 1.9 based on our analysis (Table 3), we identified four as CLAGNs from our observations. For J1150+3503, its DOT spectrum is of bad quality, suffering large uncertainties. However, since its CL transition has been reported by Wang et al. (2024), we included it in Table 2. We respectively describe the analysis and results below in Section 4.1 & 4.2 for the nine sources.

The three type 1 AGNs we observed did not show a transition from type 1 to type 2. We present analysis of their spectra in Section 4.3, and their CM diagrams are displayed in Fig. A1 in Appendix A.

To obtain measurements of the prominent emission lines, namely H α and H β , for comparison, we employed the PYTHON QSO fitting code (PYQSOFIT; Guo et al. 2018). The full-width at half maximum (FWHM), the equivalent width (EW), and the line flux of each of the two lines were obtained by fitting them with PYQSOFIT. These fitting results, along with the peak wavelength determined for each line’s broad component, are given in Table 3. Details of the spectral fitting are presented in Fig. B1–B4 in Appendix B.

For the measurements given in Table 3, the systematic uncertainties should be considered. We examined each LJT or DOT spectrum and chose several continuum regions of approximately the same flux level but different noise levels. The average fluxes of these chosen regions were calculated. We then compared these averages to that of the region with the lowest noise, and the average of their differences was adopted as the systematic uncertainty of a spectrum. Using this method, we estimated uncertainties of 13 per cent, 9 per cent, 15 per cent, and 8 per cent, respectively, for spectra of J0751+4948, J1020+2437, J1203+6053, and J1344+5126.

We estimated the mass of the black hole (BH) M_{BH} in the CLAGNs with the following formula from Vestergaard & Peterson (2006),

$$\log(M_{\text{BH}}/M_{\odot}) = \log \left[\left(\frac{\text{FWHM}(\text{H}\beta)}{\text{km s}^{-1}} \right)^2 \left(\frac{L_{5100}}{10^{44} \text{ erg s}^{-1}} \right)^{0.5} \right] + 0.91,$$

where L_{5100} is the luminosity at 5100 Å. We also estimated the Eddington ratio λ_{Edd} ($= L_{\text{bol}}/L_{\text{Edd}}$) for the accretion of a BH. For $z < 0.8$, $L_{\text{bol}} = 9.26 \times L_{5100}$, and $L_{\text{Edd}} = 1.38 \times 10^{38} M_{\text{BH}}/M_{\odot} \text{ erg s}^{-1}$ (Richards et al. 2006). In the estimation, the above systematic uncertainties were included.

4.1 Changing-look AGNs

4.1.1 J0751+4948

The optical and MIR light curves are shown in Fig. 3. A flux rise can be observed since approximately MJD 58200, with the rise in zg appearing faster. The Δzg and $\Delta W2$ values between the start of the rise and the variation peak (after MJD 59000) are $\simeq 1.1$ and $\simeq 1.3$, respectively. These variation features (cf., Fig. 1) of the source made it selected by us. The LJT spectrum, compared to the SDSS spectrum taken ~ 19 yr ago, shows broader and stronger H α emission. It also shows the emergence of an H β line, maybe an H γ line as well. To illustrate the differences, we subtracted the SDSS spectrum convolved with the LJT’s spectral resolution from the LJT spectrum, and obtained a difference spectrum. This difference spectrum is shown in Fig. 3, and the changes in H α and H β are clearly visible.

The FWHM of H β was $\simeq 3370 \text{ km s}^{-1}$ (Table 3). Using it, we obtained $M_{\text{BH}} \sim 10^{6.69} M_{\odot}$ from Eq. 1. The estimated Eddington ratio $\log \lambda_{\text{Edd}}$ was ~ -2.1 , indicating that its accretion mode was more likely the ADAF rather than the standard accretion disc flow, given the threshold of $\lambda_{\text{Edd}} \sim 0.01$ (Shakura & Sunyaev 1973; Noda & Done 2018).

4.1.2 J1020+2437

Similar to J0751+4948, the source’s zg band started brightening faster from MJD 58500 before reaching a maximum change of -1.4 mag in less than a thousand days (Fig. 4). A notable feature is that the MIR emission has been increasing since the beginning of the WISE data. Compared to the SDSS spectrum taken ~ 18 yr ago, our LJT spectrum shows a very strong H α line, accompanied with the emergence of a broad H β component. The FWHM of the strong H α line was over $10,000 \text{ km s}^{-1}$, while a similarly broad but weak H α component was required in our fitting of the SDSS spectrum. These results are consistent with that reported in Wang et al. (2024) for this source. The mass of the BH, estimated from the FWHM of the H β broad component, was $\sim 10^{8.88} M_{\odot}$. The estimated Eddington ratio $\log \lambda_{\text{Edd}}$ was ~ -1.8 .

4.1.3 J1203+6053

Compared to the other sources, flux variations of this source are more like that of a flickering type, with no major brightening event. Carefully examining the multi-band light curves, there seemed to be a sudden increase starting from \sim MJD 59200 in the optical, possibly accompanied by a delayed jump in the MIR bands (Fig. 5). The DOT spectrum suffers large uncertainties and only captures half of the H α line. We did not obtain a difference spectrum for this source. In any case, the presence of broad H α and H β (as well as H γ)

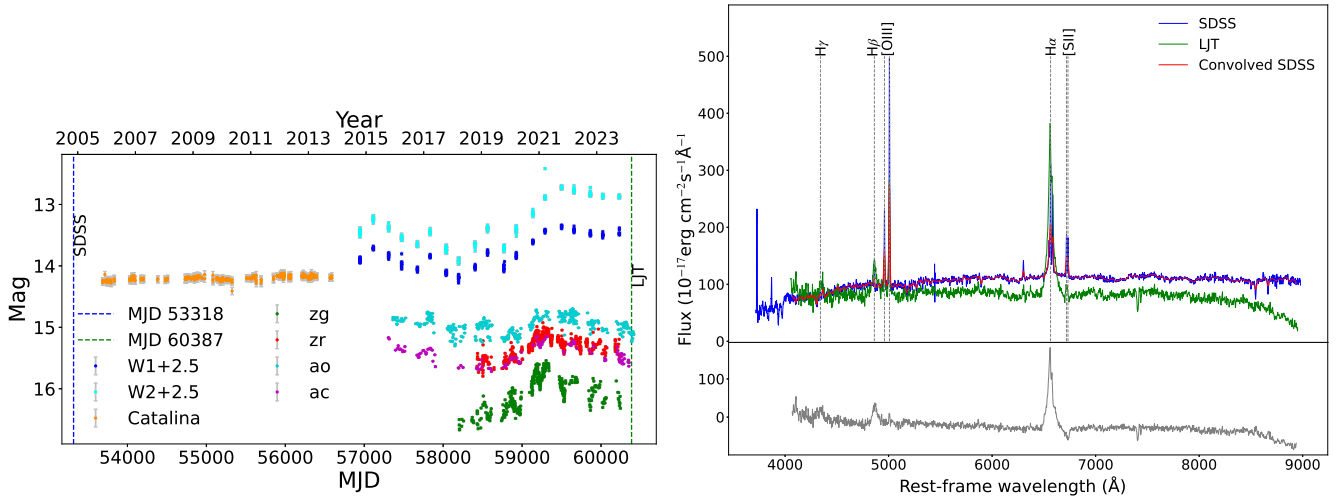


Figure 3. Optical and MIR light curves (*left*) and spectra (*right*) of J0751+4948. Two vertical dashed lines in the left panel mark the observation times of the SDSS and LJT spectra shown in the right upper panel. The two spectra are vertically shifted for clarity. In the *right lower* panel, a difference spectrum between the two spectra is shown.

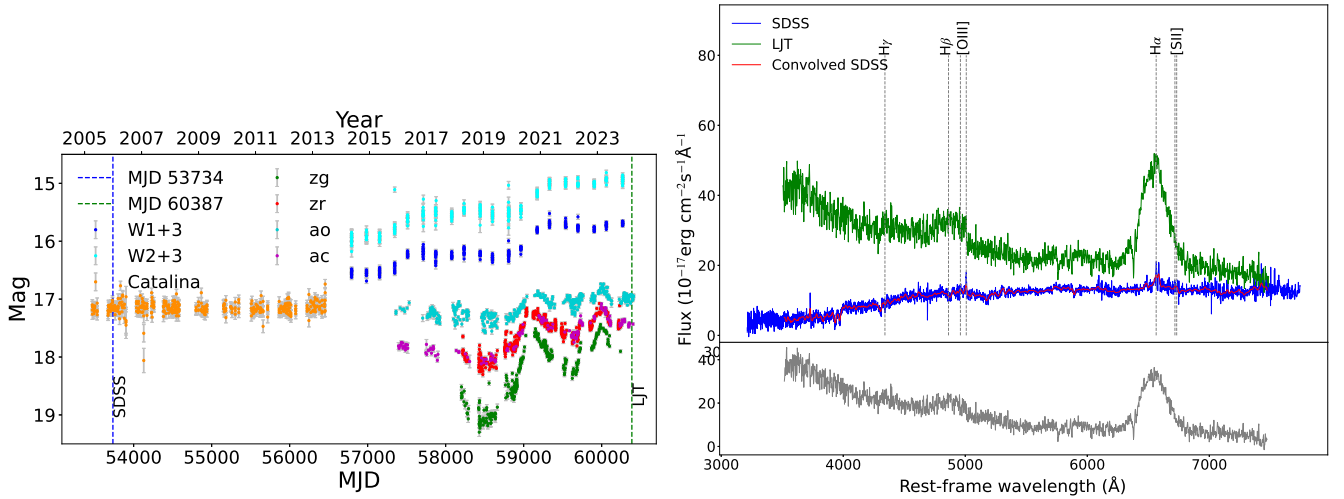


Figure 4. Same as Fig. 3 for J1020+2437.

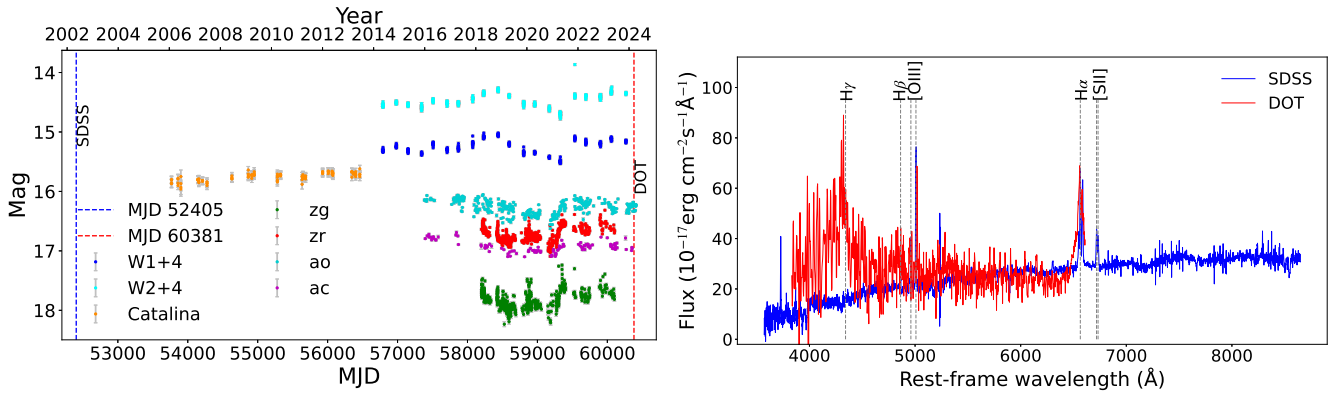


Figure 5. Same as Fig. 3 for J1203+6053, but because the DOT spectrum is noisy, no difference spectrum for it is obtained and shown.

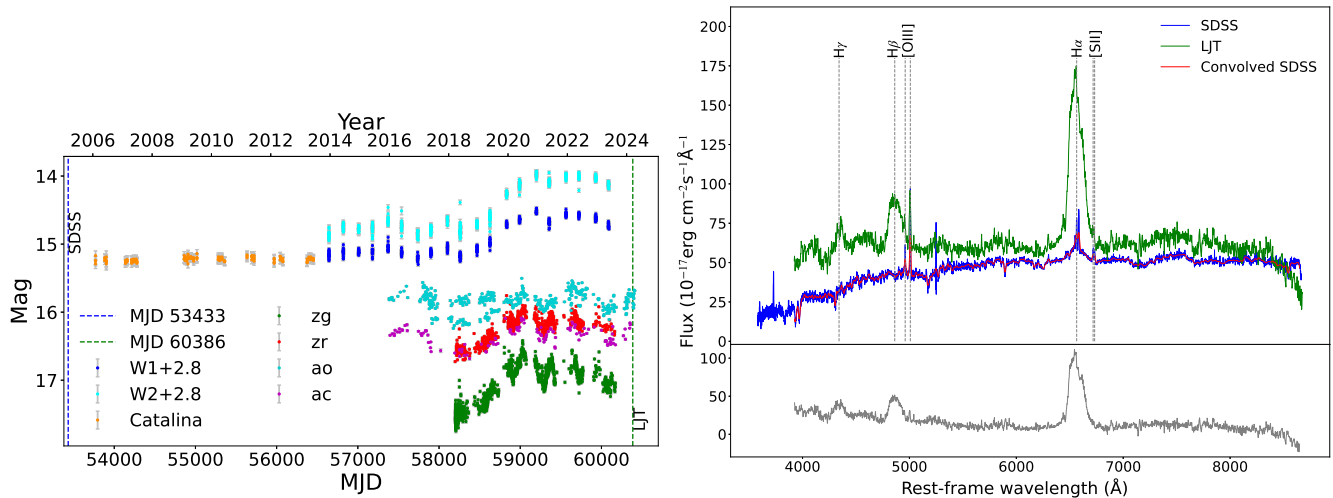


Figure 6. Same as Fig. 3 for J1344+5126.

components, as opposed to their absence in the SDSS spectra, suggests this is a CLAGN. The BH mass was estimated to be $\sim 10^{7.97} M_{\odot}$, although this value is highly uncertain due to the limited quality of the spectrum. The estimated Eddington ratio $\log \lambda_{\text{Edd}}$ was ~ -1.97 .

4.1.4 J1344+5126

This source, similar to J1020+2437, exhibited a <1000 day long optical flux increase (peaking around MJD 59000), a long-term brightening in the MIR bands, and significant spectral changes (Fig. 6). For the latter, our LJT spectrum shows not only the appearances of strong and broad H α and H β lines, but also the certain appearance of an H γ line. The turn-on of a H γ line has not been commonly seen in AGNs exhibiting the H β turn-on phenomenon. In addition, some weak absorption features were possibly detected in the SDSS spectrum, suggesting a relatively strong contribution from the host galaxy to the observed emission at the time. The BH mass was $\sim 10^{7.55} M_{\odot}$, and the Eddington ratio $\log \lambda_{\text{Edd}}$ was ~ -2.4 . Further investigation of this source’s general properties is warranted in order to draw a full picture of this AGN’s dramatic activity.

4.2 Other targets

We did not detect CL transitions from type 2 to type 1 in the other four targets selected from the BWB pattern. No significant variations of the emission lines were seen in the spectra we obtained, as compared to the respective SDSS spectra. In the Appendix Fig. C1, we show their light curves. Comparing the light curves to those of CLAGNs in Section 4.1, we also see larger zg (or bluer) flux variations, but the amplitudes are smaller. For example, all Δzg (and Δzr) values are less than 0.9 mag. In addition, the MIR light curves are either relatively flat (as in J1053+4929) or have been decaying recently (as in the other three sources). These differences will be considered in our follow-up work when selecting targets as CLAGN candidates. The further selection consideration will then be tested.

4.3 Type 1 AGNs

We also tested to select type 1 AGNs with negative k values as the targets, and to check if they would have a transition from type 1 to type 2 based on the CM property. In addition, their zr -band fluctuations were small, with an amplitude of ~ 0.2 mag (Fig. A1). However, the LJT spectra did not show any significant spectral changes compared to the respective SDSS spectra (Fig. 7). These cases may indicate that AGNs could stay stable, without showing any significant variations, for a long time period of ~ 2000 day. Further consideration to improve our selection for the turn-off transition will be taken.

5 DISCUSSION AND SUMMARY

As suggested in Zhu et al. (2024), the BWB pattern seen in CM diagrams of type 2 AGNs may be used to find CLAGNs with transitions from type 2 to type 1. We thus carried out a test observation run and observed nine selected targets. Among them, two have already been identified as CLAGNs in Wang et al. (2024), and three are newly discovered by us. The success rate is greater than 50 per cent if we only consider our small sample. Comparing the light curves of the sample, the apparent differences between CLAGNs and non-CLAGNs are that the latter had smaller magnitude changes (< 0.9 mag in zg ; Table 1) and most of them also had decaying MIR emissions in recent years (Fig. C1). By contrast, the CLAGNs all had > -1.0 mag flux increases in zg , which were mostly due to a brightening flare-like event (except J1203+6053). Such events are not seen in the non-CLAGNs (Fig. C1); they instead showed flicker-like variations. Moreover, the CLAGNs showed accompanying MIR brightening. We note that among the four CLAGNs we observed, J0751+4948 and J1344+5126 had $W1 - W2$ colour changes from < 0.5 (galaxy-like) to > 0.5 (AGN-like; e.g., López-Navas et al. 2023a) when they entered their flare-like brightening phase, while the other two sources had the colours always > 0.5 . The MIR activity and the related colour changes could be a critical indicator to reflect the optical variations (and thus the accretion rate changes; Sheng et al. 2017) and to be applied in finding CLAGNs (Sheng et al. 2020). Given the differences, which can be veri-

Table 3. Measurements of H α and H β lines from the fitting with PYQSOFIT for the four CLAGNs

Line	(J0751) SDSS	LJT	(J1020) SDSS	LJT
H α broad				
FWHM	3350 \pm 170	3858 \pm 66	9500 \pm 730	10750 \pm 270
EW	218.5 \pm 4.7	11620 \pm 29	142 \pm 15	362.2 \pm 5.2
Flux	1773 \pm 38	12670 \pm 320	319 \pm 35	8860 \pm 130
Peak	6562.21 \pm 0.87	6563.65 \pm 0.74	6547.9 \pm 5.9	6540.7 \pm 3.3
H α narrow				
FWHM	302.6 \pm 3.6	766 \pm 27	354 \pm 16	0
EW	161.1 \pm 2.0	310 \pm 13	24.4 \pm 1.4	0
Flux	1306 \pm 16	3380 \pm 140	54.5 \pm 3.1	0
H β broad				
FWHM	0	3370 \pm 240	0	8720 \pm 780
EW	0	190 \pm 17	0	46.1 \pm 5.5
Flux	0	3080 \pm 270	0	1430 \pm 170
H β narrow				
FWHM	353.8 \pm 1.9	752 \pm 53	0	0
EW	22.50 \pm 0.79	21.6 \pm 9.5	0	0
Flux	273.7 \pm 9.6	350 \pm 150	0	0
MJD	53318	60387	53734	60387
log(M_{BH}/M_{\odot})	...	6.96 $^{+0.17}_{-0.20}$...	8.88 $^{+0.13}_{-0.14}$
log(λ_{Edd})	...	-2.11 \pm 0.18	...	-1.84 \pm 0.15
Line	(J1203) SDSS	DOT	(J1344) SDSS	LJT
H α broad				
FWHM	0	8020 \pm 240	7650 \pm 220	8870 \pm 570
EW	0	325.1 \pm 9.1	371 \pm 12	1141 \pm 43
Flux	0	5780 \pm 130	1122 \pm 36	1728 \pm 64
Peak	0	6575.4 \pm 2.1	6555.7 \pm 2.5	6551.1 \pm 2.2
H α narrow				
FWHM	430.5 \pm 7.7	610 \pm 21	299.5 \pm 8.2	604 \pm 75
EW	155.5 \pm 3.1	19.37 \pm 0.94	46.6 \pm 2.6	46.6 \pm 6.9
Flux	382.9 \pm 7.6	361 \pm 18	140.4 \pm 7.9	72 \pm 11
H β broad				
FWHM	0	5593.9 \pm 4.5	0	5599.6 \pm 5.1
EW	0	33.7 \pm 1.7	0	87.2 \pm 3.2
Flux	0	874 \pm 44	0	390 \pm 15
H β narrow				
FWHM	450.8 \pm 7.5	0	357.8 \pm 7.6	820 \pm 130
EW	10.1 \pm 1.2	0	4.5 \pm 1.1	9.4 \pm 3.1
Flux	41.8 \pm 4.9	0	16.8 \pm 4.0	41 \pm 13
MJD	52405	60381	53433	60386
log(M_{BH}/M_{\odot})	...	7.97 $^{+0.16}_{-0.18}$...	7.55 $^{+0.16}_{-0.15}$
log(λ_{Edd})	...	-1.97 \pm 0.20	...	-2.41 \pm 0.10

FWHM, EW, flux, and peak (wavelength) are in units of km s $^{-1}$, angstrom (\AA), 10^{-17} erg cm $^{-2}$ s $^{-1}$, and angstrom (\AA), respectively.

fied from observations of more sources, in addition to the simple BWB pattern, factors such as optical and MIR magnitude changes, as well as the association with a major brightening event should be considered in our selection method. Hopefully with more observations, we would be able to establish the criteria for more effectively selecting CLAGN candidates. We note that the results, in-turn, would allow us to configure the general properties of CLAGNs.

Our method is similar to those focusing on different aspects of AGNs. Besides the mentioned MIR-variation method, for example, Wang et al. (2024) were able to successfully find CLAGNs among sources showing a mismatch between variabilities and previously-classified types. Our test to find type 1 to type 2 transitions follow the same idea. However, the failures (although only with three of the observed sources) suggests more factors should be included in addition to the minimum variations in our selection. López-Navas et al.

2022 employed a machine-learning classification tool to select type 1 AGNs among previously classified type 2 ones, and had a success rate of ≥ 66 per cent in finding CLAGNs. The classification tool should have considered all aspects of AGNs, including optical variations and related CM behaviours as mentioned in our method. In comparison, our method is simple and probably more direct. Physically, large BWB slopes caused by significant flux changes (for example, $\Delta z_g > -1.0$ mag in our cases) likely indicate strong variations due to significant accretion rate changes; the colour variability and magnitude variability in the optical and MIR are more likely to exclude the variable obscuration scenario (see, e.g., Yang et al. 2018 for detailed discussion). We are planning a more complete study by carrying out spectroscopy of a large sample. We will focus more on whether there is a flare-like event in association with the BWB variations. The results will possibly allow us to refine the selection criteria and es-

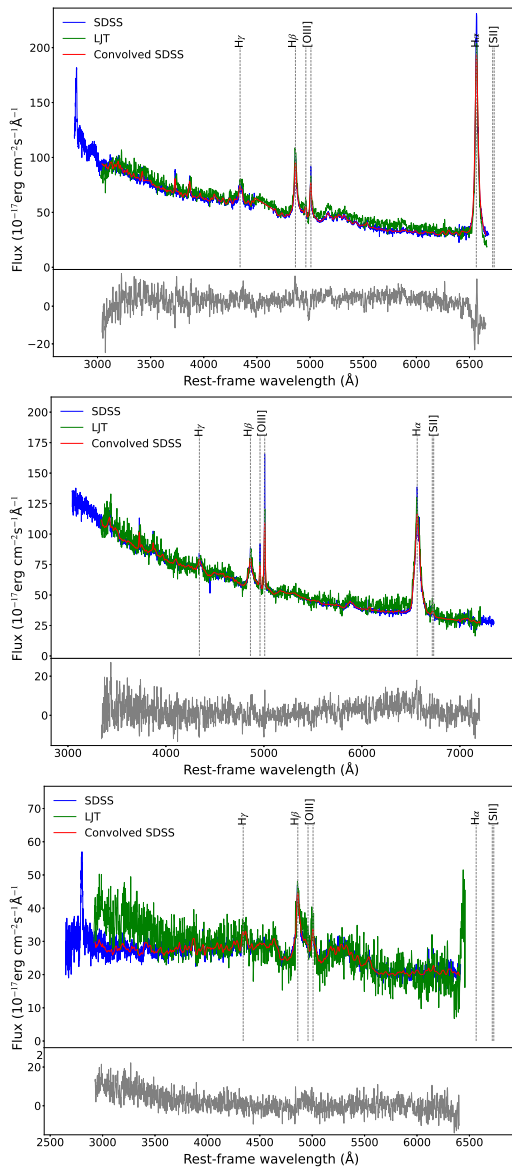


Figure 7. Spectra of three type 1 AGNs we tested, displayed from *top to bottom*: J1127+2654, J1527+2233, and J1606+2903. For each source, a difference spectrum is made and shown.

establish some characteristics of CLAGNs for their variability aspect.

It has been summarized from analyses of large samples of CLAGNs that their Eddington ratios tend to be around 10^{-2} , in a range of $\log \lambda_{\text{Edd}}$ from -2.5 to -1.0 (Zelty et al. 2024; Panda & Śniegowska 2024). The four CLAGNs observed by us all had $\log \lambda_{\text{Edd}}$ in this range. As $\lambda_{\text{Edd}} \sim 10^{-2}$ is a transition point for the accretion mode from the ADAF to the standard thin disc, the λ_{Edd} properties could indicate that the CL phenomenon is caused by the mode transition, probably in the inner region close to the BH in order to match the short CL timescales (Noda & Done 2018).

Among the four CLAGNs observed by us, J1344+5126 had the lowest $\log \lambda_{\text{Edd}}$ value (~ -2.4). It can be noted that in its SDSS spectrum, weak absorption features were present. CLAGNs with similar spectra were detected in studies such as reported by MacLeod et al. (2016b), Ruan et al. (2016)

and Yang et al. (2018). This type of spectra suggests a weak AGN emission component in the sources at the time. In fact, based on our fitting to the SDSS spectra of the four CLAGNs (Fig. B1–B4), the host-galaxy emission components were strong or dominant. For such cases, J. Li et al. (in preparation) have conducted simulation calculations, and according to their study, the cause of the apparent CL phenomenon could be due to significant short-term changes in the extreme ultraviolet (EUV) radiation of an AGN, which is part of the overall flux fluctuations caused by disc temperature turbulences (Cai et al. 2018). The EUV radiation affects the strengths of the BELs. At the weak phase of the EUV radiation, the influence of the host galaxy often results in characteristics typical of type 1.8/1.9 or even type 2, yet intrinsically, the BELs are consistently present. In other words, the CLAGNs in our cases (except J1203+6053) had a broad H α component in their SDSS spectra, and they were mostly type 1.9, not pure type 2. The upward brightening fluctuation naturally has a BWB pattern, which accompanies the ‘turn-on’ of the BELs. Thus, this strongly varied EUV-radiation scenario may provide an alternative explanation for the CL phenomenon.

As a summary, we employed the CM patterns, suggested in Zhu et al. (2024), for selecting CLAGN candidates among previously-classified type 2 AGNs in the SDSS. We observed nine candidates, four of which were confirmed to display the CL phenomenon in our observations and one of which was identified by Wang et al. (2024) as the spectrum we obtained from it was of bad quality. We also tested to extend the selection method to previously-classified type 1 AGNs, but none of the three observed sources showed a transition to type 2. The results prove that this rather simple method can effectively find CLAGNs, while the failure cases suggest the selection criteria could be refined. We plan to carry out observations of a large number of possible candidates, which aim to not only identify CLAGNs, but also draw lines on the properties of the optical/MIR variations and related CM changes between CLAGNs and non-CLAGNs. The program will possibly provide quantified characteristics for CLAGNs, and help us gain a full understanding of this particular phenomenon.

ACKNOWLEDGEMENTS

This work was based on observations obtained with the Samuel Oschin Telescope 48-inch and the 60-inch Telescope at the Palomar Observatory as part of the Zwicky Transient Facility project. ZTF is supported by the National Science Foundation under Grant No. AST-2034437 and a collaboration including Caltech, IPAC, the Weizmann Institute for Science, the Oskar Klein Center at Stockholm University, the University of Maryland, Deutsches Elektronen-Synchrotron and Humboldt University, the TANGO Consortium of Taiwan, the University of Wisconsin at Milwaukee, Trinity College Dublin, Lawrence Livermore National Laboratories, and IN2P3, France. Operations are conducted by COO, IPAC, and UW.

This work made use of data products from the Wide-field Infrared Survey Explorer, which is a joint project of the University of California, Los Angeles, and the Jet Propulsion

Laboratory/California Institute of Technology, funded by the National Aeronautics and Space Administration.

We thank the anonymous referee for detailed insightful comments, which greatly helped improve the manuscript. This research is supported by the Basic Research Program of Yunnan Province No. 202201AS070005, the National Natural Science Foundation of China (12273033), and the Original Innovation Program of the Chinese Academy of Sciences (E085021002). L.Z. acknowledges the support of the science research program for graduate students of Yunnan University (KC-24249083).

DATA AVAILABILITY

The data underlying this article will be shared on reasonable request to the corresponding author.

REFERENCES

- Ahumada R., et al., 2020, *ApJS*, **249**, 3
- Antonucci R., 1993, *ARA&A*, **31**, 473
- Aretxaga I., Joguet B., Kunth D., Melnick J., Terlevich R. J., 1999, *ApJ*, **519**, L123
- Bellm E. C., et al., 2019, *PASP*, **131**, 018002
- Cai Z.-Y., Wang J.-X., Zhu F.-F., Sun M.-Y., Gu W.-M., Cao X.-W., Yuan F., 2018, *ApJ*, **855**, 117
- Cohen R. D., Rudy R. J., Puetter R. C., Ake T. B., Foltz C. B., 1986, *ApJ*, **311**, 135
- Denney K. D., et al., 2014, *ApJ*, **796**, 134
- Dexter J., Begelman M. C., 2019, *MNRAS*, **483**, L17
- Dong Q., Zhang Z.-X., Gu W.-M., Sun M., Zheng Y.-G., 2024, *arXiv e-prints*, p. [arXiv:2408.07335](https://arxiv.org/abs/2408.07335)
- Drake A. J., et al., 2009, *ApJ*, **696**, 870
- Eracleous M., Halpern J. P., 2001, *ApJ*, **554**, 240
- Feng J., Cao X., Li J.-w., Gu W.-M., 2021, *ApJ*, **916**, 61
- Frederick S., et al., 2019, *ApJ*, **883**, 31
- Gezari S., et al., 2017, *ApJ*, **835**, 144
- Graham M. J., et al., 2020, *MNRAS*, **491**, 4925
- Green P. J., et al., 2022, *ApJ*, **933**, 180
- Guo H., Shen Y., Wang S., 2018, PyQSOFit: Python code to fit the spectrum of quasars, *Astrophysics Source Code Library*, record ascl:1809.008 (ascl:1809.008)
- Guo W.-J., et al., 2024a, *arXiv e-prints*, p. [arXiv:2408.00402](https://arxiv.org/abs/2408.00402)
- Guo W.-J., et al., 2024b, *ApJS*, **270**, 26
- Katebi R., et al., 2019, *MNRAS*, **487**, 4057
- Kumar B., et al., 2018, *Bulletin de la Societe Royale des Sciences de Liege*, **87**, 29
- LaMassa S. M., et al., 2015, *ApJ*, **800**, 144
- Lawrence A., 1987, *PASP*, **99**, 309
- López-Navas E., et al., 2022, *MNRAS*, **513**, L57
- López-Navas E., et al., 2023a, *MNRAS*, **524**, 188
- López-Navas E., et al., 2023b, *MNRAS*, **524**, 188
- MacLeod C. L., et al., 2016a, *MNRAS*, **457**, 389
- MacLeod C. L., et al., 2016b, *MNRAS*, **457**, 389
- Mereghetti S., et al., 2021, *Experimental Astronomy*, **52**, 309
- Noda H., Done C., 2018, *MNRAS*, **480**, 3898
- Panda S., Śniegowska M., 2024, *ApJS*, **272**, 13
- Planck Collaboration et al., 2020, *A&A*, **641**, A6
- Ricci C., Trakhtenbrot B., 2022, *arXiv e-prints*, p. [arXiv:2211.05132](https://arxiv.org/abs/2211.05132)
- Richards G. T., et al., 2006, *ApJS*, **166**, 470
- Ross N. P., et al., 2018, *MNRAS*, **480**, 4468
- Ross N. P., Graham M. J., Calderone G., Ford K. E. S., McKernan B., Stern D., 2020, *MNRAS*, **498**, 2339
- Ruan J. J., et al., 2016, *ApJ*, **826**, 188
- Ruan J. J., Anderson S. F., Eracleous M., Green P. J., Haggard D., MacLeod C. L., Runnoe J. C., Sobolewska M. A., 2019, *ApJ*, **883**, 76
- Runnoe J. C., et al., 2016, *MNRAS*, **455**, 1691
- Shakura N. I., Sunyaev R. A., 1973, *A&A*, **24**, 337
- Shappee B. J., et al., 2014, *ApJ*, **788**, 48
- Sheng Z., Wang T., Jiang N., Yang C., Yan L., Dou L., Peng B., 2017, *ApJ*, **846**, L7
- Sheng Z., et al., 2020, *ApJ*, **889**, 46
- Śniegowska M., Czerny B., Bon E., Bon N., 2020, *A&A*, **641**, A167
- Stern D., et al., 2018, *ApJ*, **864**, 27
- Storchi-Bergmann T., Baldwin J. A., Wilson A. S., 1993, *ApJ*, **410**, L11
- Tadhunter C., 2008, *New Astron. Rev.*, **52**, 227
- Tohline J. E., Osterbrock D. E., 1976, *ApJ*, **210**, L117
- Tonry J. L., et al., 2018, *PASP*, **130**, 064505
- Trakhtenbrot B., et al., 2019, *ApJ*, **883**, 94
- Urry C. M., Padovani P., 1995, *PASP*, **107**, 803
- Vestergaard M., Peterson B. M., 2006, *ApJ*, **641**, 689
- Wang C.-J., et al., 2019, *Research in Astronomy and Astrophysics*, **19**, 149
- Wang J., Zheng W. K., Brink T. G., Xu D. W., Filippenko A. V., Gao C., Xie C. H., Wei J. Y., 2023, *ApJ*, **956**, 137
- Wang S., et al., 2024, *ApJ*, **966**, 128
- Winkler H., 1992, *MNRAS*, **257**, 677
- Wright E. L., et al., 2010, *AJ*, **140**, 1868
- Yang Q., et al., 2018, *ApJ*, **862**, 109
- Zelty G., et al., 2022, *ApJ*, **939**, L16
- Zelty G., et al., 2024, *ApJ*, **966**, 85
- Zhu L.-T., Li J., Wang Z., Zhang J.-J., 2024, *MNRAS*, **530**, 3538

APPENDIX A: COLOUR-MAGNITUDE DIAGRAMS OF THREE TYPE 1 AGNS

APPENDIX B: SPECTRUM FITTING WITH PYQSOFIT

APPENDIX C: LIGHT CURVES OF FOUR TYPE 2 AGNS

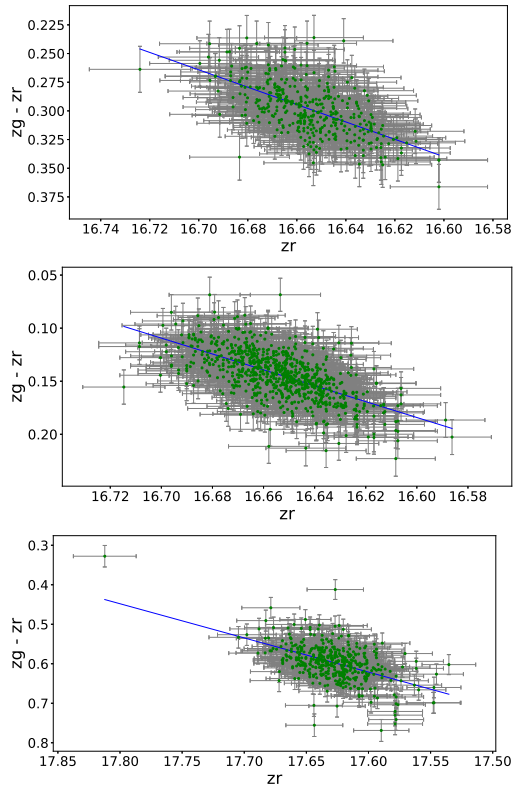


Figure A1. *Top to bottom:* colour-magnitude diagrams of type 1 AGN J1127+2654, J1527+2233, and J1606+2903. Their k values were respectively -0.758 ± 0.001 , -0.749 ± 0.001 , and -0.865 ± 0.001 , and zr -band variations were less than 0.2 mag (excluding one outlier in J1606+2903).

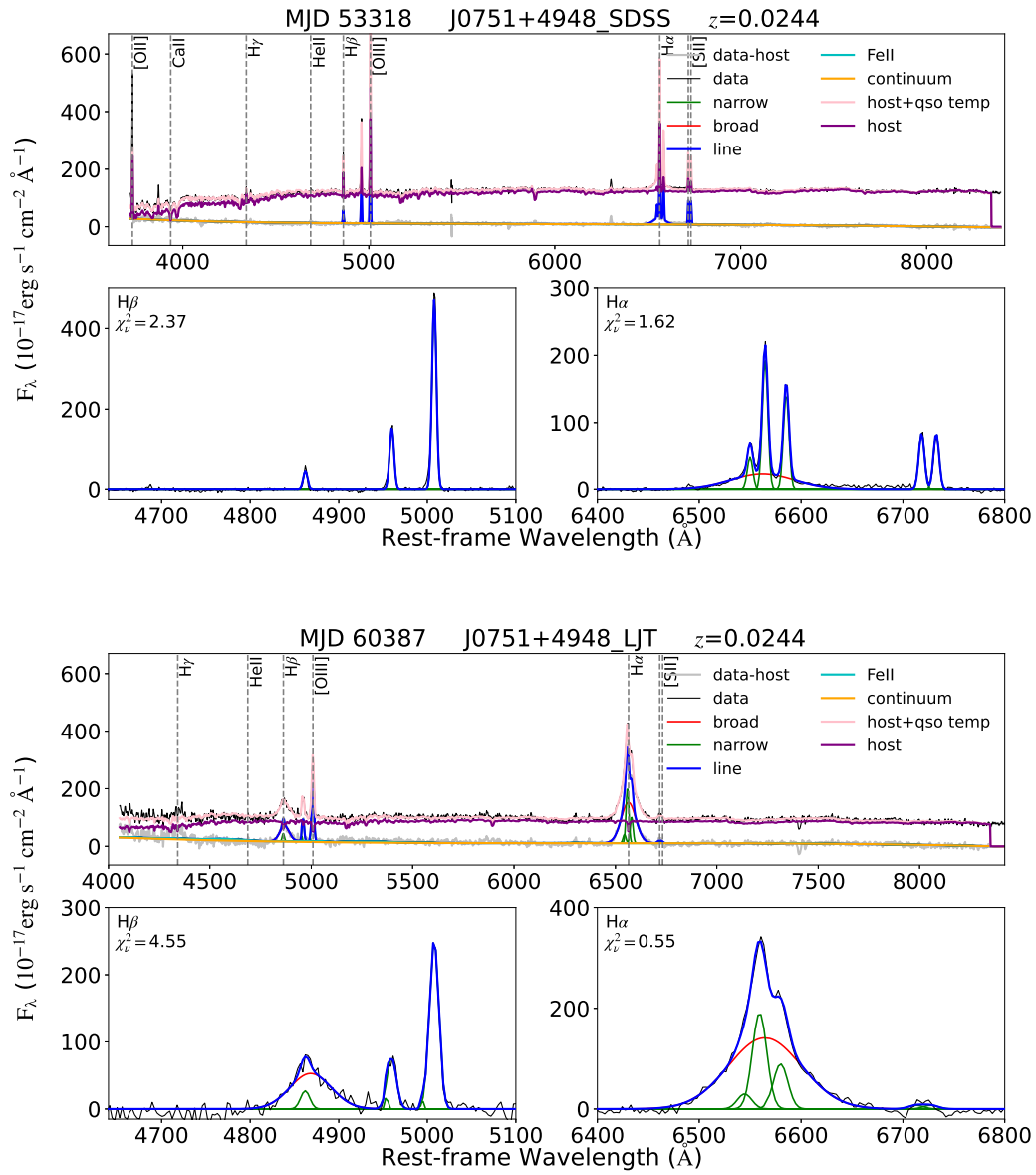


Figure B1. J0751+4948

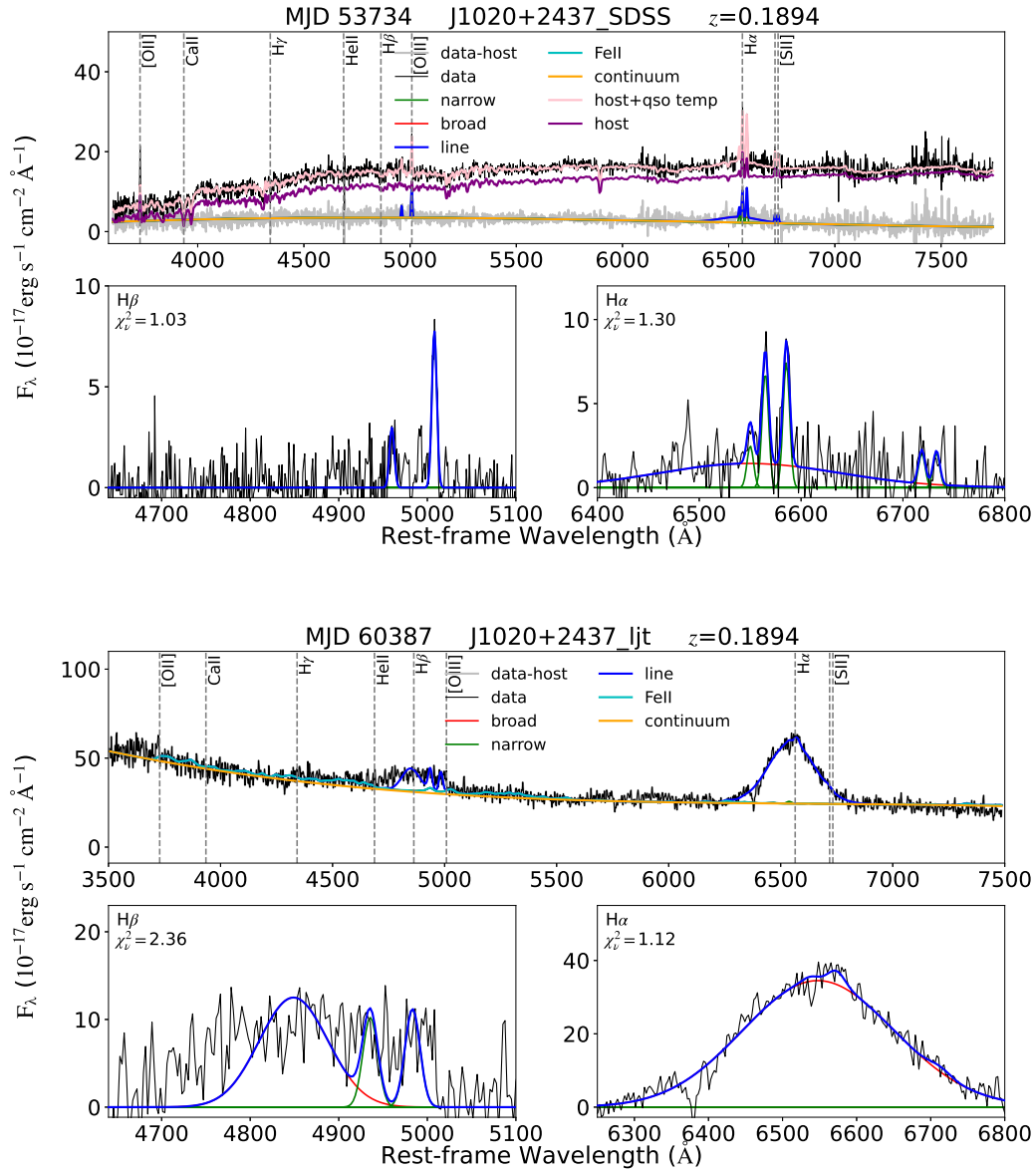


Figure B2. J1020+2437

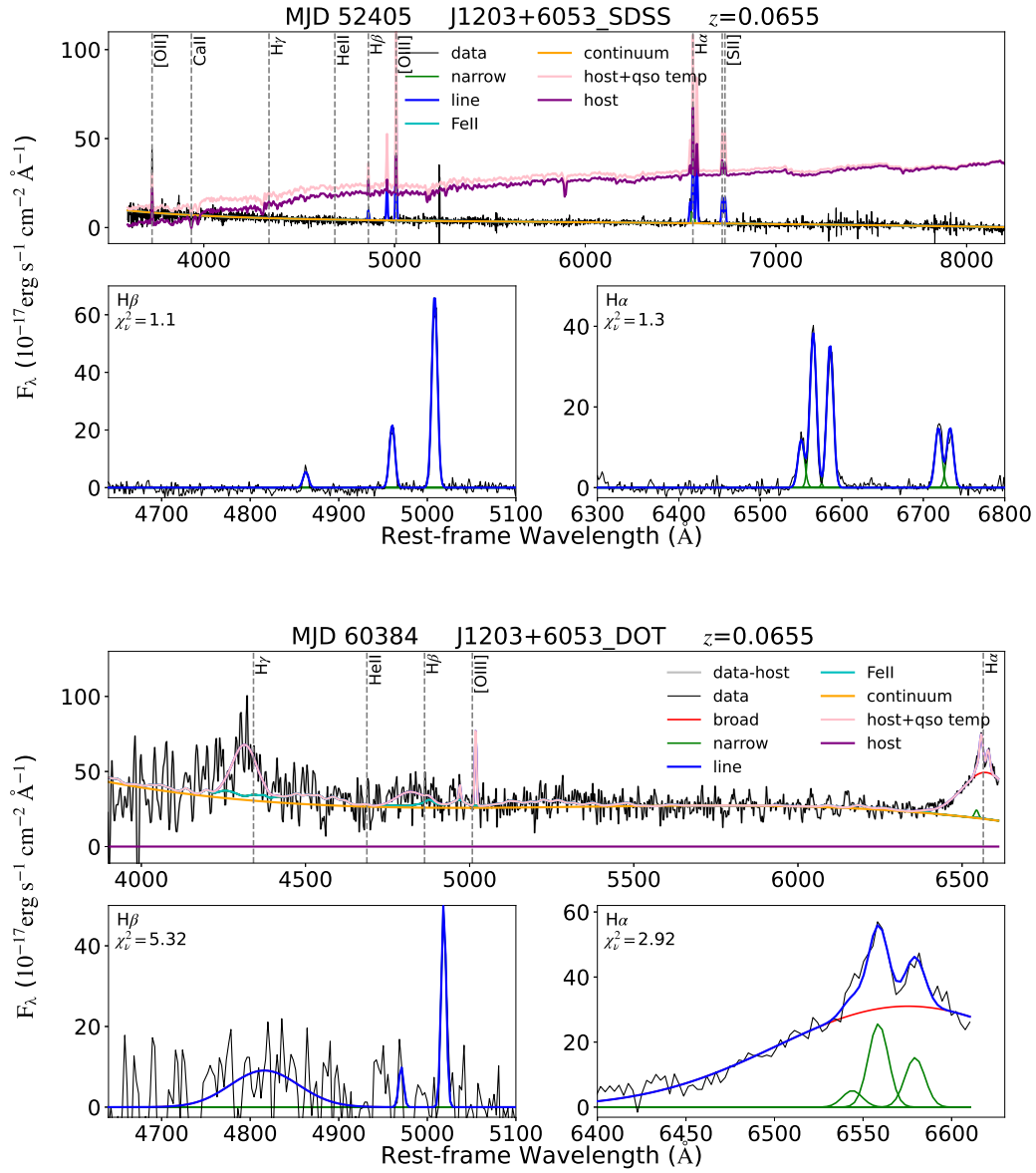


Figure B3. J1203+6053

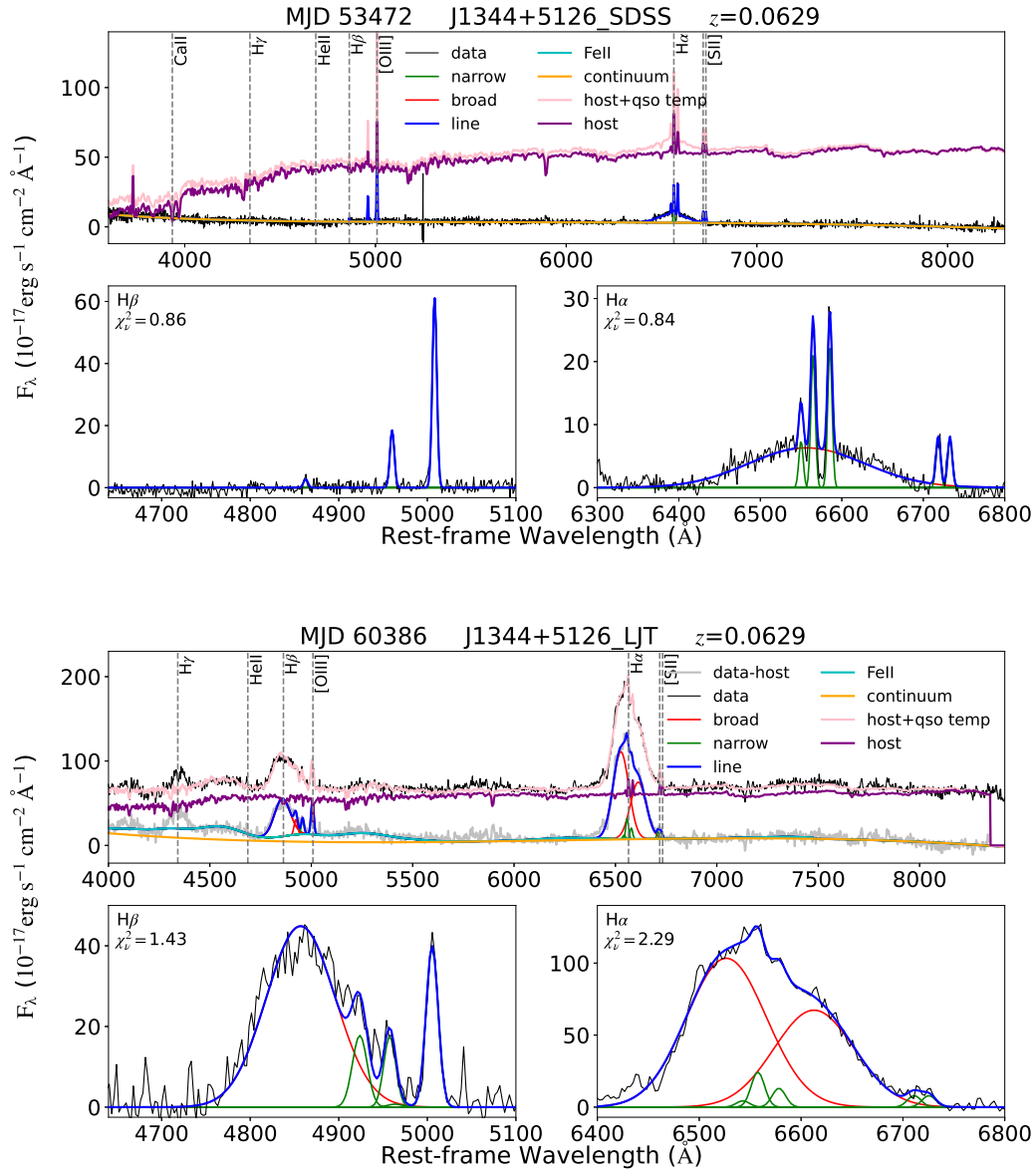


Figure B4. J1344+5126

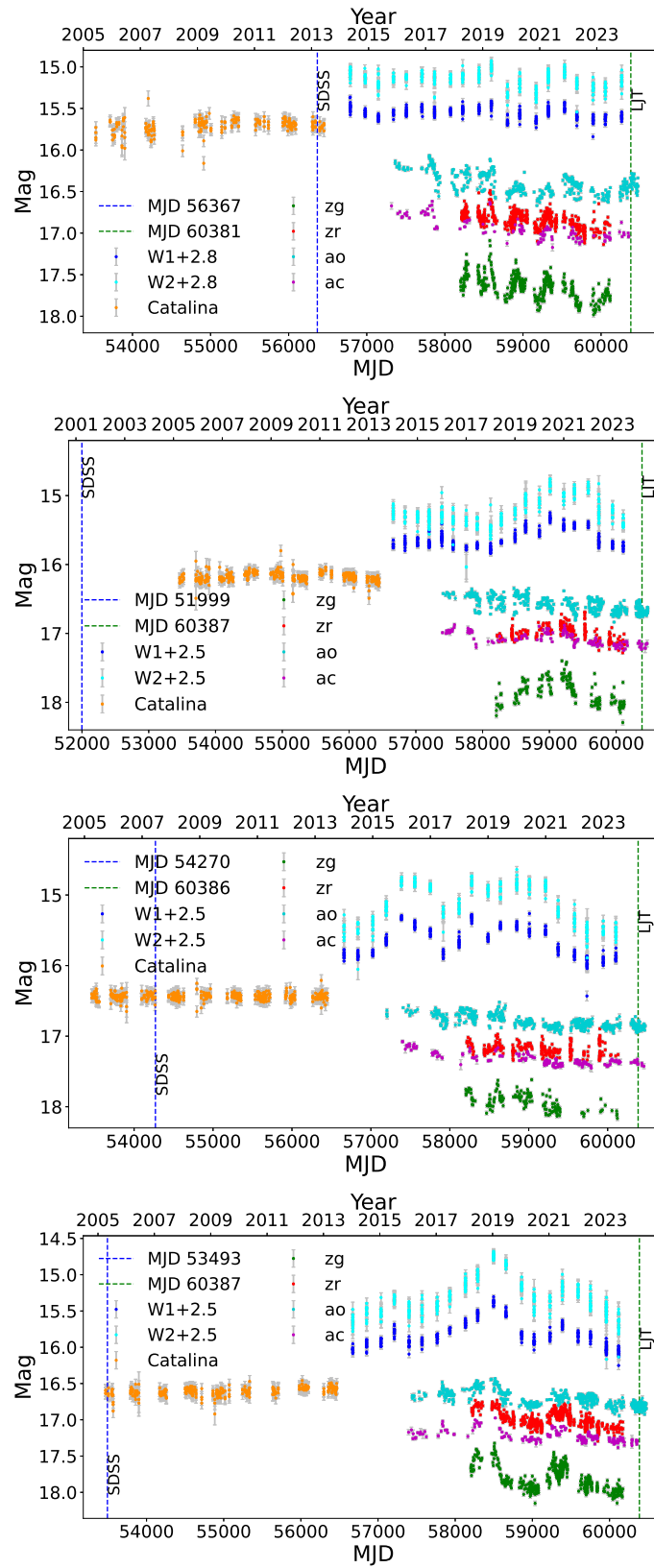


Figure C1. *Top to bottom:* light curves of J1053+4929, J1246-0156, J1252+0717, and J1423+2454.